

Mixed Hydrate Nucleation: Molecular Mechanisms and Cage Structures

Lei Wang, Kyle Hall, Zhengcai Zhang, and Peter G. Kusalik*



Cite This: *J. Phys. Chem. B* 2022, 126, 7015–7026



Read Online

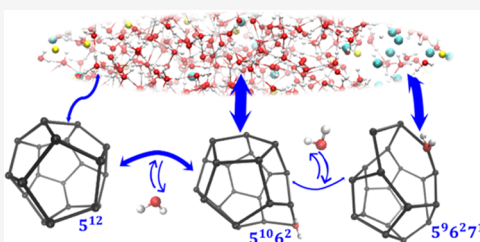
ACCESS |

Metrics & More

Article Recommendations

Supporting Information

ABSTRACT: The molecular-level details of the formation of mixed gas hydrates remain elusive despite their significance for a variety of scientific and industrial applications. In this study, extensive molecular simulations have been performed to examine the behavior of CH₄/H₂S mixed hydrate nucleation utilizing two different simulation setups varying in compositions and temperatures. The observed behavior exhibits similar phenomenology across the various systems once differences in nucleation rates and guest uptake are accounted for. We find that CH₄ is always enriched in the hydrate phase while the aqueous phase is enriched in H₂S. Even with H₂S as a minor component (i.e., 10% mole fraction), the system can mirror the overall nucleation kinetics of pure H₂S hydrate systems with CH₄-dominant nuclei. Through analyses of cages and their transitions, nonstandard cages, particularly those with 12 faces (e.g., 5¹⁰6²), have been found to be key intermediate cage types in the early stage of nucleation. Additionally, we present previously unreported cage types comprising heptagonal faces (e.g., 5⁹6²7¹) as having a significant role in the early-stage gas hydrate structural transitions.



INTRODUCTION

Gas hydrates are ice-like clathrate substances in which water molecules form hydrogen-bonded cages containing gas molecules. Many types of small molecules, such as methane, ethane, propane, carbon dioxide, THF, and hydrogen sulfide, can be guests in hydrates.^{1–4} Depending on the properties (e.g., size, shape, and polarizability) of different guest molecules, different types of hydrate crystal structures can be formed at various pressures and temperatures.^{1–4} There are two hydrate structures that are most common: structure I (sI) and structure II (sII). For example, pure CH₄, H₂S, C₂H₆, and CO₂ prefer to form sI hydrates, which consists of 5¹² and 5¹²6² cages. Some larger molecules (e.g., propane, isobutane, and THF) prefer to form sII hydrates, which consists of 5¹² and 5¹²6⁴ cages, where these guests occupy only the latter cages, while some smaller molecules (e.g., H₂, and N₂) tend to form sII by occupying both cages.

There is a great deal of interest in understanding the mechanisms of gas hydrate nucleation given a wide range of hydrate-related applications in sustainable technologies and other applications, including but not limited to CO₂ sequestration,^{2,4} gas separation,^{5–7} water desalination,^{7,8} natural gas hydrate mining,⁹ and flow assurance of the oil/gas transportation.^{2,10} A majority of the hydrate-based techniques involve the formation of mixed gas hydrates. For instance, in hydrate-based CO₂ sequestration processes, other gases, such as N₂, H₂, or CH₄, are likely to be present and can be hydrate formers.^{2,5,7} The sour natural gas found in oil/gas fields and transportation contains H₂S and CO₂ and should give rise to mixed gas hydrates.⁶ Thus, there is a significant need to elucidate the microscopic details of mixed gas hydrate

nucleation, particularly the roles of different guest molecules, to facilitate the control of hydrate formation and the development of hydrate-based technologies.

Despite the relevance of the mixed guests to gas hydrate-based applications,² an understanding at the molecular level of the roles of different guest molecules in mixed hydrate nucleation has remained elusive. Since hydrate nucleation is very challenging to investigate experimentally given the stochastic nature of nucleation and the temporal and spatial length scales involved, molecular simulations have become a prime tool to study molecular mechanisms.¹¹ In recent studies, molecular dynamics (MD) simulations have been widely used to explore nucleation behavior for a wide range of guests. Most of these studies have focused on a single guest molecule (e.g., CH₄,^{12–28} H₂S,^{29,30} CO₂,³¹ C₂H₆,³² C₃H₈,³³ ethylene oxide,³⁴ THF,³⁵ and generic guests^{36,37}), while a limited number of studies have been reported on mixed hydrate systems (e.g., CH₄/CO₂,³⁸ CH₄/H₂S,^{39–41} CH₄/THF,⁴² and mixed light hydrocarbons⁴³) despite their scientific and technological significance. The nucleation process in mixed gas hydrates has been reported to be essentially analogous to that in the pure guest system.^{40,43} Yet, because of different properties of the guest species, the molecular details of mixed hydrate

Received: May 9, 2022

Revised: August 12, 2022

Published: September 1, 2022



nucleation are complex and far from being understood. For instance, a small amount of another hydrocarbon species (i.e., C_2H_6 ⁴³, C_3H_8 ⁴³ or 2,2-dimethylbutane⁴⁴) in methane can significantly enhance the nucleation rate of methane hydrates by stabilizing early structural fluctuations in the solution. Unlike these hydrocarbons, only a high content of CO_2 (> 75%) in a CH_4/CO_2 mixture was found to accelerate the nucleation rate relative to pure CH_4 systems, while cages occupied by CO_2 are prevalent.³⁸

The nucleation of mixed CH_4/H_2S hydrate is an industrially and scientifically relevant process due to the vast natural gas reservoir and hydrate-bearing sediment reserves with H_2S present.^{45,46} A minor component of H_2S in the vapor phase can cause the H_2O (L)/hydrate/vapor three-phase coexistence line to shift significantly to higher temperatures and lower pressures compared to that of pure CH_4 guest hydrate.^{6,47–50} Such unexpected stabilization of the H_2S -containing hydrates can be used as an effective method for the separation of H_2S and, on the other hand, can bring huge flow assurance challenges and considerable costs in hydrate-related production, transportation, and processing. However, there is a paucity of studies exploring CH_4/H_2S hydrate nucleation at the molecular level. Hall et al⁴⁰ proposed that CH_4/H_2S mixed hydrate nucleation (within timescales of 100 ns) is comparable to pure H_2S under the same conditions (250 K and 50 MPa).²⁹ In this previous study,⁴⁰ CH_4 -rich nuclei forming from a H_2S -rich aqueous solution were observed in a heterogeneous aqueous system with a 50/50 molar ratio of CH_4/H_2S . Zhang et al⁴³ compared the impacts of different guests and compositions on mixed hydrate nucleation in a homogeneous aqueous solution with an overall fixed guest mole fraction of 0.048 at 10 MPa and 260 K. They reported that for their systems, CH_4/H_2S mixed hydrate nucleation rarely occurred in timescales of hundreds of nanoseconds when the content of H_2S was > 25%.

This previous work has generated the following questions: (1) how do different compositions of CH_4/H_2S affect the molecular-level mechanistic details of mixed hydrate nucleation and (2) how do the different physical system setups (i.e., homogeneous and heterogeneous) impact the hydrate nucleation. To address these questions, the current study utilizes two systems. A system where a CH_4/H_2S nanobubble is immersed in an aqueous solution is investigated with various relative ratios of the two guest species. In this circumstance, the nucleation process of the mixed hydrate is the net of the effects of the transfer of guest molecules from the nanobubble into the aqueous solution and the abilities of the guest molecules to be enclathrated. We also examine CH_4/H_2S mixed hydrate nucleation in a homogenous aqueous solution with the same initial concentration for both guests. The impact of temperature on the mixed hydrate nucleation is explored. As the nucleation proceeds in absence of a second (guest species) phase, there is a depletion of the amount of guests in the aqueous solution. We consistently find that the CH_4 species is always enriched in hydrate phases relative to that of liquid phases across the two different systems. According to detailed analyses of hydrate cages, we find that nonstandard cages tend to initiate the emergence of the order and dominate during the early stages of nucleation from the aqueous phase. Our results highlight the key roles of nonstandard cages, particularly cages with 12 faces (e.g., $S^{10}6^2$ and S^86^4 cages), in the apparent pathway for the formation of the hydrate structure, thereby furthering the understanding of nucleation behavior of mixed

hydrates. In addition, we have identified that the cages containing a small number of heptagonal faces (e.g., S^96^{27}) play an important role in the structural transitions during early-stage hydrate formation.

METHODS

Two systems, system A (sys-A) and system B (sys-B), have been employed. Sys-A is a two-phase system where a small CH_4/H_2S nanobubble was immersed in an aqueous solution. Sys-B is a single-phase system where CH_4 and H_2S molecules were randomly distributed within an aqueous solution (see Figure 1). Our primary motivation for examining nucleation

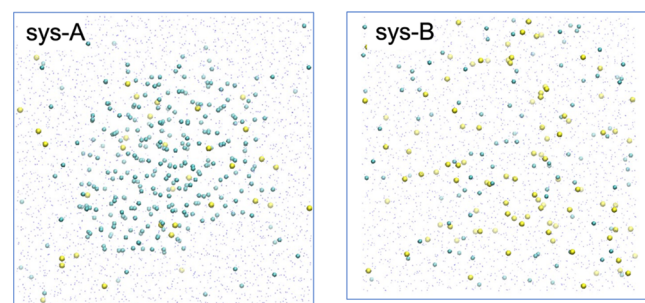


Figure 1. Representative initial configurations with a CH_4 composition of 90% ($y_{CH_4} = 90\%$) for sys-A (left) and of 50% ($y_{CH_4} = 50\%$) for sys-B (right). Liquid water molecules are displayed by blue dots. The yellow and cyan spheres represent H_2S and CH_4 molecules, respectively.

behavior with two different system setups is to demonstrate that the results obtained are generally robust with respect to the details of system setup, specific models, and conditions. We define the gas composition in the CH_4/H_2S mixture systems as y_i and the gas concentration (mole fraction) in solution as x_i (where i can be either CH_4 or H_2S , or both species).

Sys-A was generated with an initial CH_4/H_2S nanobubble in liquid water, where various gas compositions ($y_{CH_4} = 50, 75$, and 90%) with a total of 340 guest molecules and 3035 H_2O molecules were considered. This physical setup gives an overall gas mole fraction of 0.10 for sys-A. The configurations of sys-A were initially equilibrated at 300 K and 50 MPa for 100 ns, then sequentially quenched to 290, 280, and 270 K for 10, 10, and 20 ns, respectively. Once at 270 K, the velocities for all molecules were randomized to produce 10, 20, and 20 independent trajectories with $y_{CH_4} = 50, 75$, and 90% , respectively. These independent trajectories were then cooled to 240 K for 200 ns long production runs. For sys-A, the H_2O was represented with the TIP4P/2005 potential,⁵¹ and the Lennard-Jones cross terms were determined using geometric combining rules. Additional details for the simulation used for sys-A are the same as those in refs 39–41.

Sys-B is a homogeneous solution with 100 CH_4 , 100 H_2S , and 2944 H_2O molecules, giving an initial guest mole fraction in the solution of 0.0636. The initial configuration of sys-B was equilibrated for 2 ns at 300 K and 10 MPa, then 5, 10, and 10 independent production trajectories were followed at 260, 265, and 270 K, respectively. The production runs for sys-B range from 500 to 800 ns, depending on the time required for nucleation and growth to occur. The H_2O was modeled by the TIP4P/Ice potential,⁵² and the Lennard-Jones cross terms were obtained by Lorentz–Berthelot mixing rules for sys-B.⁵³

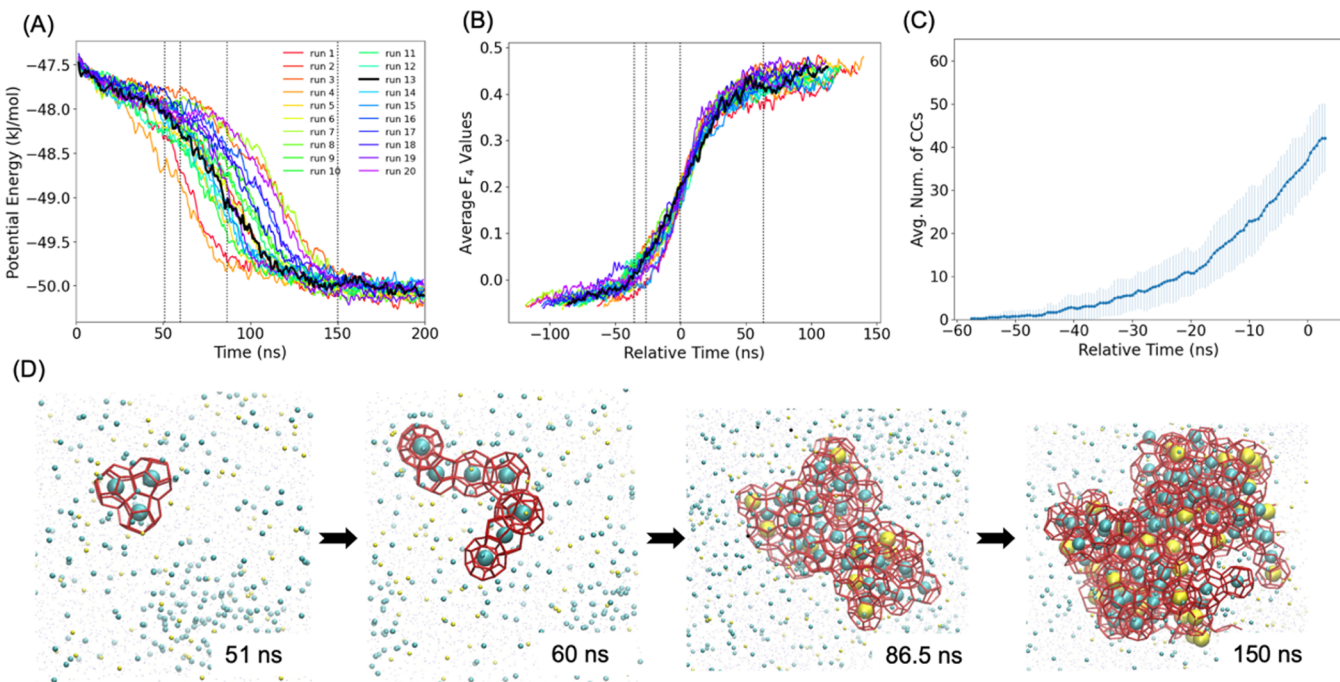


Figure 2. Hydrate nucleation process of mixed gas hydrate systems for sys-A with y_{CH_4} of 75%. (A) Time evolution of the potential energy for each run. (B) Temporally aligned average F_4 curves for the 20 nucleating runs according to their inflection points. The color pattern in panel (A) is also applied in panel (B). (C) Number of complete cages (CCs) temporally aligned and averaged over the set of nucleating trajectories. The error bars representing standard deviations are provided. (D) Snapshots from the nucleation process in a representative trajectory, run 13. The CCs in the largest cluster are connected by red tubes. H₂S and CH₄ within this cluster are shown as yellow and cyan spheres, respectively. Liquid water molecules are blue dots, and smaller yellow and cyan spheres represent H₂S and CH₄ molecules in solution. The dashed lines in panels (A) and (B) correspond to the time points of the snapshots in panel (D).

Additional details of the methods used in the simulations for sys-B are the same as those in ref 43.

For both sys-A and sys-B, CH₄ was modeled with a single Lennard-Jones united atom,⁵⁴ and H₂S was modeled by the four-site model proposed by Forester et al.⁵⁵ Note that both TIP4P/Ice and TIP4P/2005 potentials are refined TIP4P water models that can give a reasonable description of the phase equilibrium.^{51,52} Applying the two water potentials to sys-A and sys-B allows nucleation to be observable at different temperatures on a simulation timescale and enables the temperature for both systems to be about 10 K below the ice melting temperature of the corresponding water models being employed.^{52,56} These model combinations have been used in several previous simulation-based gas hydrate studies.^{39–41,57,58} Extensive sets of MD simulations were performed within NPT ensemble.

The F_4 order parameter (which has average values of -0.4, -0.04, and 0.7 for ice, liquid water, and gas hydrate, respectively)⁵⁹ was used to monitor hydrate nucleation. A modified version of FSICA (face-saturated incomplete cage analysis), allowing for the detection of cages that include seven-member rings, was used to detect the hydrogen-bonded cages and corresponding occupancies.⁶⁰ For structure analysis and for detecting cage transitions, 10 ps average configurations were used.⁶¹ Results presented in this work are based on a 1 ns rolling average of the data sets unless stated otherwise. The error bars representing standard deviations were calculated from the set of nucleating trajectories for each condition. The details of the different models used in this study are tabulated in Table S1, and estimates for the melting temperatures (T_m)

of ice and gas hydrates for these models are tabulated in Table S2.

RESULTS AND DISCUSSION

To examine the underlying mechanisms of the mixed hydrate nucleation, we have detected and tracked details of the nucleation process using the average F_4 values and cage formation as detected by FSICA. Briefly, FSICA defines two types of cages: (1) complete cages (CCs) and (2) incomplete cages (ICs). Every vertex in the former cage type (CC) is shared with at least three edges; otherwise, cages detected by FSICA are ICs.⁶⁰ We find that cages containing multi-occupancy are rare in the present systems in accord with previous studies of mixed hydrate nucleation.⁴⁰ Consequently, singly occupied cages were the focus of the analyses herein. Given the stochastic characteristic of the hydrate nucleation, temporal alignments were used to generate averages over trajectories^{39–41} that allow the comparison of nucleation behavior across various conditions in the current study. Temporal alignment of nucleating trajectories is achieved by setting the time corresponding to the inflection point in the time dependence of the average F_4 order parameter equal to zero, which yields relative times, t_{relative} (see Figure 2B). The time $t_{\text{relative}} = 0$ in this time frame represents the fastest ordering in the system as captured by the F_4 values. It is apparent that nucleation occurs when $t_{\text{relative}} < 0$ and the aligned F_4 curves are well overlapped. We find that the average number of CCs measured in the t_{relative} is also well aligned (i.e., see Figure 2C) at times consistent with the F_4 curves indicating the formation of the new hydrate phase. As the early stage of

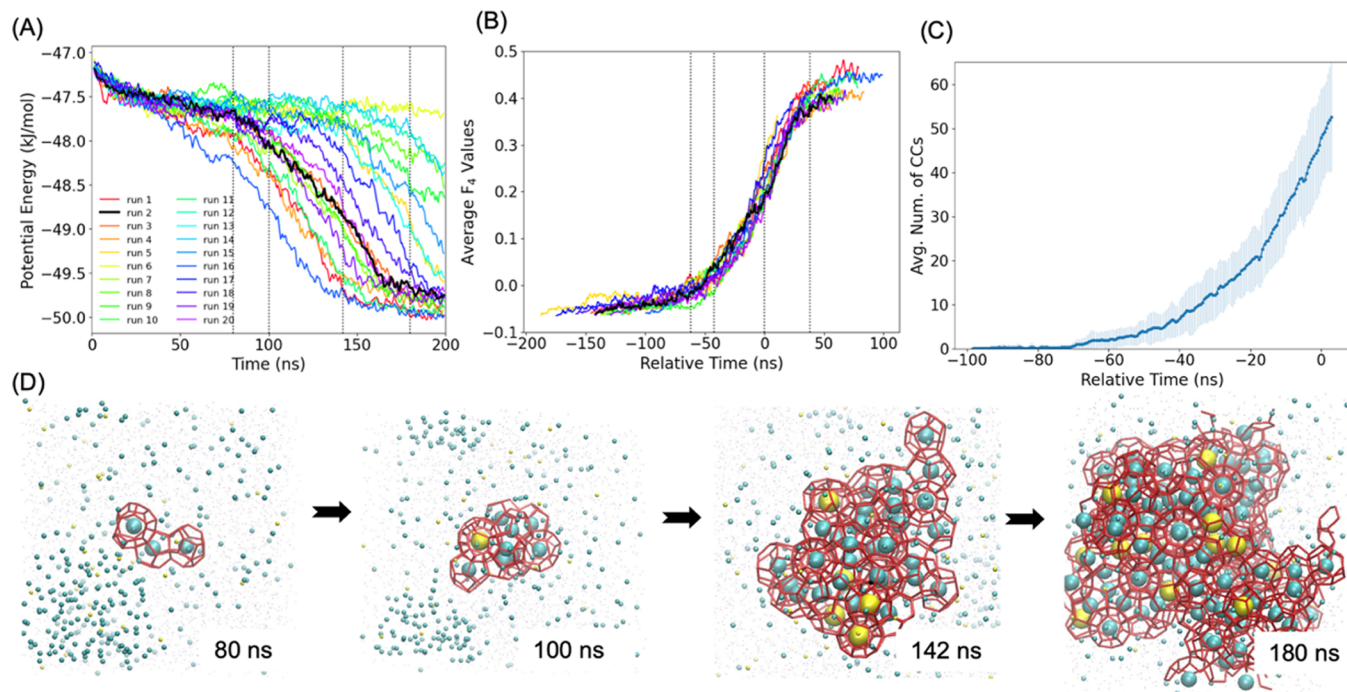


Figure 3. Hydrate nucleation process of mixed gas hydrate systems for sys-A with y_{CH_4} of 90%. (A) Time evolution of the potential energy for each run. (B) Temporally aligned average F_4 curves for the 13 nucleating runs according to their inflection points. The color pattern in panel (A) is also applied in panel (B). (C) Number of complete cages (CCs) temporally aligned and averaged over the set of nucleating trajectories. The error bars representing standard deviations are provided. (D) Snapshots from the nucleation process in a representative trajectory, run 2. The molecules are represented and colored using the same pattern as those in Figure 2D. The dashed lines in panels (A) and (B) correspond to the time points of the snapshots in panel (D).

nucleation is the focus of this study, the remaining analyses will be focused on the $t_{\text{relative}} < 0$ regimes.

Our detailed analyses for the nucleation process will focus on sys-A. For a given trajectory, as shown in Figure 2 with $y_{\text{CH}_4} = 75\%$, decreases in potential energy along with increases of average F_4 values essentially coincide with the appearance of a small cluster of complete cages (CCs). The hydrate nucleus snapshots provided in Figure 2D for run 13 from various stages of the simulation coincide with the black curves in Figure 2A,B. At 51 ns in the trajectory for run 13, a CC cluster with three cages occupied by CH_4 molecules initially forms. The system then undergoes further growth of this hydrate nucleus. At $t_{\text{relative}} = 0$, the size of the cluster has grown to around 40 CCs.

The results from the sys-A with different compositions of guests show similar behavior for nucleation (see Figures 3 and S1). The nucleation behavior observed in Figure 3 with an increased y_{CH_4} of 90% is slower, where only 13 out of 20 trajectories have nucleated after 200 ns. In Figure 3D, we see the appearance of the largest CC cluster with three CH_4 -occupied cages at 80 ns, then the nucleus proceeds to grow. Due to the high content of CH_4 ($y_{\text{CH}_4} = 75$ or 90%) in the systems, the CH_4 -filled cages are unsurprisingly prevalent in the nuclei (see Figures 2D and 3D). The impact of the composition will be further detailed below.

The hydrate nucleation processes and molecular configurations taken from various stages of the representative simulations of sys-B are presented in Figures S2–S4. Comparing to the behavior shown in sys-A (see Figure S1), we find that nucleation with the same $y_{\text{CH}_4} = 50\%$ is slower in sys-B with greater variation in nucleation times (as detailed in

the SI). For example, in Figure S2D where the representative snapshots capture the hydrate nucleation at 270 K, we see that the largest cluster exhibits large fluctuations in size and shape, and consequently, for times up to 260 ns, the number of CCs making up the largest CC cluster continues to vary. Small values of average F_4 and the number of CCs in the system in Figure S2B,C again imply that systems are undergoing structural fluctuations during that time. We conjecture that the slower growth and larger fluctuations exhibited by sys-B arise in part because of the low guest concentration relative to that in the hydrate, which is further depleted locally as nucleation proceeds. This is in contrast to sys-A where its nanobubble can serve as a guest reservoir and may also act as a heterogeneous nucleation site.

In general, the nucleation processes of sys-B are comparable to those of sys-A. However, comparing the nucleation process of sys-A with $y_{\text{CH}_4} = 50\%$ and that of sys-B at 260 K (as presented in Figures S1 and S4), with the same initial gas composition, $y_{\text{CH}_4} = 50\%$, and similar relative supercooling of the H_2O models, we see that with a lower concentration and no gas reservoir in sys-B, the progressive growth of the nuclei is slower and the system suffers from larger structural fluctuations in the surrounding aqueous phase, although nucleation for both cases occurs reasonably rapidly, for example, as indicated by decreases of the potential energies. Using the same models as those in sys-B, a previous study of gas hydrates in a homogeneous solution with $\text{CH}_4/\text{H}_2\text{S}$ observed no nucleation events occurring in H_2S -rich solutions ($y_{\text{H}_2\text{S}} \geq 75\%$) and only 2 out of 10 nucleating trajectories with $y_{\text{H}_2\text{S}} = 50\%$ within 500 ns at 260 K and 10 MPa.⁴³ We remark that the total

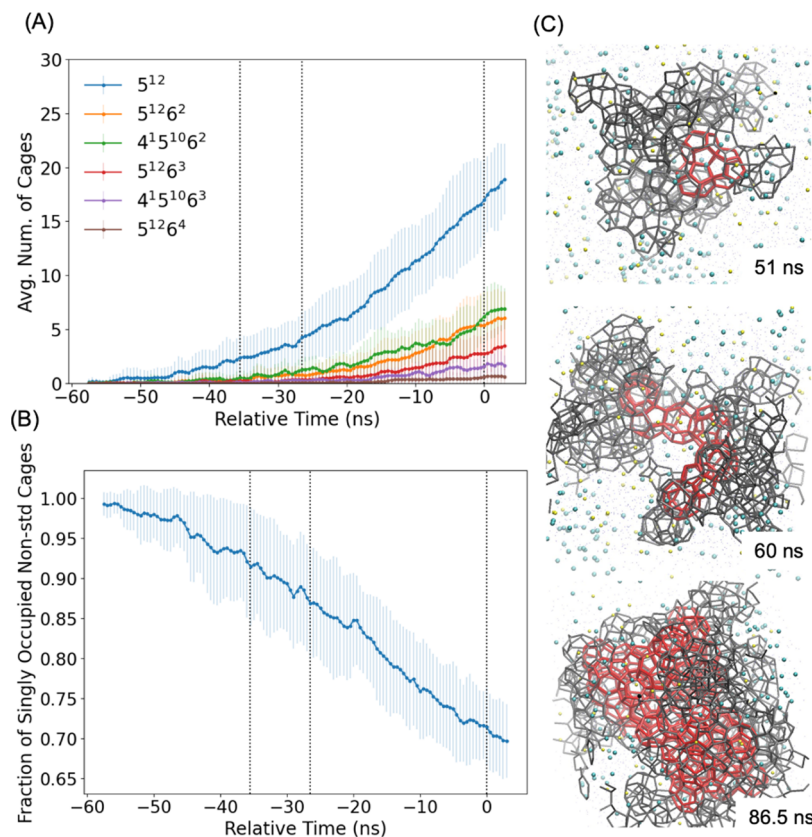


Figure 4. Structures of hydrate nuclei in sys-A with $y_{\text{CH}_4} = 75\%$. (A) Average numbers of several important standard (std) cages during the nucleation. (B) Fraction of singly occupied cages that are nonstandard (nonstd) cages. In panels (A) and (B), the error bars representing standard deviations are provided. (C) Snapshots taken from the same run as in Figure 2D showing the largest cluster comprised of std cages (red tube) and nonstd cages (gray tube). Liquid water molecules are displayed by blue dots, and yellow and cyan spheres represent H_2S and CH_4 molecules in solution, respectively. Guest molecules within cages are omitted for clarity. The dashed lines in panels (A) and (B) correspond to the relative times of the snapshots in panel (C).

concentration in this previous work (0.048)⁴³ is lower than that of sys-B (0.0636). Thus, the elevated total concentration of the gas molecules has enhanced the nucleation rate of these mixed gas hydrates.

In previous studies,^{14,16,26,31–33,38–40,62} a set of cages ($5^{12}6^n \cdot 4^15^{10}6^m$, where $n = 0, 2, 3$, and $m = 2, 3, 4$) have been the focus of their analyses and are reported as being essential for the formation of gas hydrate nuclei. This set of cages is usually known as “standard” (std) cages, where all other cages are then nonstandard (nonstd) cages. We note that the set of std cages is a subset of complete cages (CCs).⁶⁰ To further elucidate the nucleation process, Figure 4A shows the trend of dominant std cages during the early stage of nucleation in sys-A with $y_{\text{CH}_4} = 75\%$. The order of the relative populations of the std cages is consistent with previous studies⁶² with 5^{12} appearing first and being most prevalent, then $5^{12}6^2$, $4^{15}106^2$, followed by $5^{12}6^3$, $4^{15}106^3$, $5^{12}6^4$. The cage $4^{15}106^4$ is not presented as it is rarer than $5^{12}6^4$.

As can be seen in Figure 4B, nonstd cages are, on average, the overwhelming majority among the singly occupied cages appearing transiently when the system is still in its quiescent period (i.e., the time when the number of std cages is close to zero (see Figure 4A) and the average F_4 value is close to -0.04 (see Figure 2B)). As the hydrate nucleus begins to grow, the percentage of nonstd cages decreases somewhat, although they still dominate in the system. Additionally, we can see in Figure 4C that the std cages tend to be near the center of the cluster

while the nonstd cages tend to be in the interfacial area between the hydrate phase (std-cage region) and the aqueous phase. This behavior associated with nonstd cages is consistent with previous studies.^{40,42} We conjecture that the formation of these nonstd cages, which are somewhat disordered and asymmetric, appears to be kinetically favored as there are lower entropy penalties associated with their formation. In general, the trend of std cages and both percentage and locations of nonstd cages in the system are comparable across the different compositions for sys-A and the different temperatures for sys-B (see Figures S6–S10).

The hydrate structures formed in this study generally have a relatively low level of crystallinity, as indicated by (1) a small value for the ratio of $5^{12}6^2/5^{12}$ cages (which is three in sI hydrates) and (2) significant numbers of nonstd cages. Yet, these hydrate structures could be expected to anneal if the simulation timescales were significantly extended.¹⁴ The above observations support a two-step mechanism of the hydrate nucleation¹⁴ which features the initial formation of a more amorphous structure that subsequently anneals.

We next turn to the important question of how the composition of the aqueous phase impacts that of the hydrate phase. Since 5^{12} cages are dominant in the set of std cages, the analysis for the composition of hydrate nuclei will focus on 5^{12} and nonstd cages. As shown in Figure 5, the number of CH_4 -filled cages exceeds that of H_2S -filled cages for both 5^{12} and nonstd cages. This is consistent with the CH_4 -rich aqueous

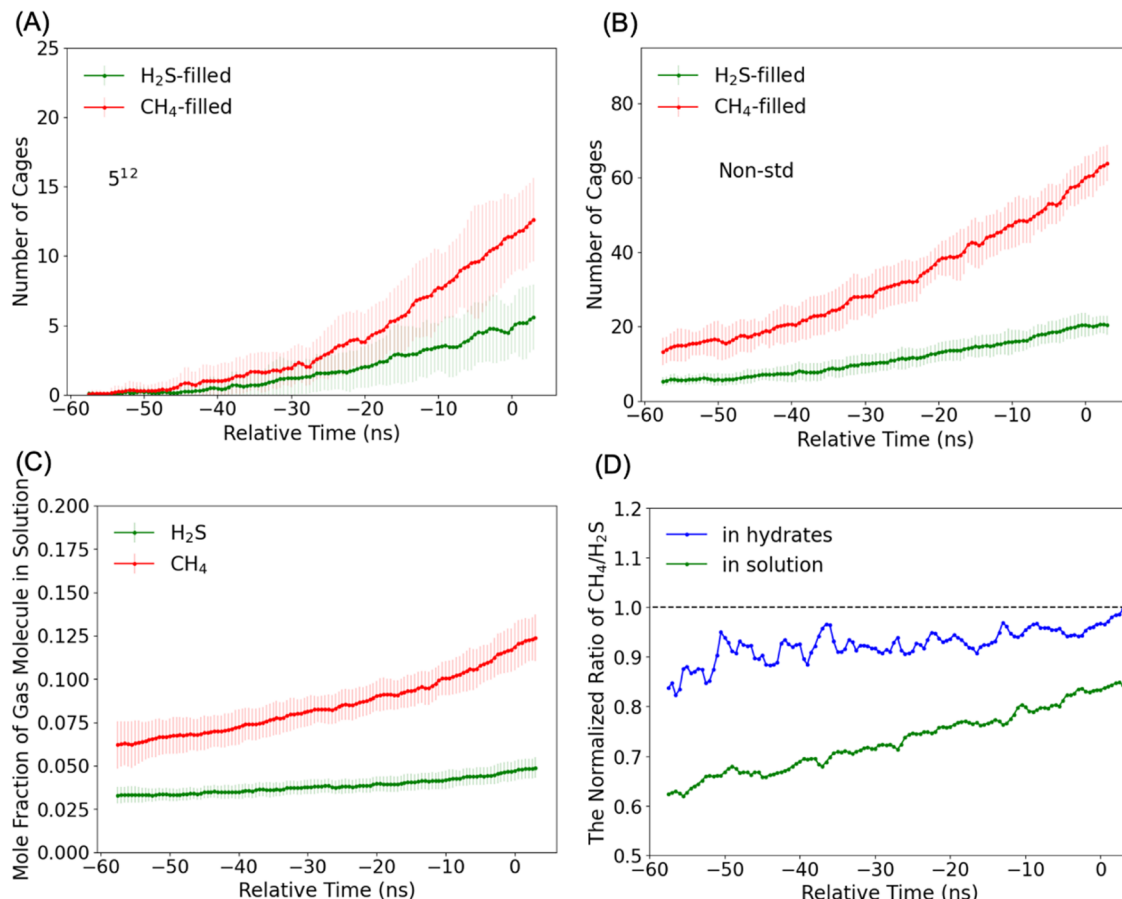


Figure 5. Composition of the hydrate nuclei in sys-A with y_{CH_4} of 75%: (A) for 5^{12} cages, (B) for all nonstd cages, and (C) in the aqueous phase. (D) Normalized ratio of $\text{CH}_4/\text{H}_2\text{S}$ in the hydrate nuclei and the aqueous phase, where the value has been normalized by the overall ratio of $\text{CH}_4/\text{H}_2\text{S} = 3$ (i.e., since y_{CH_4} of 75%). In panels (A)–(C), the error bars representing standard deviations are provided.

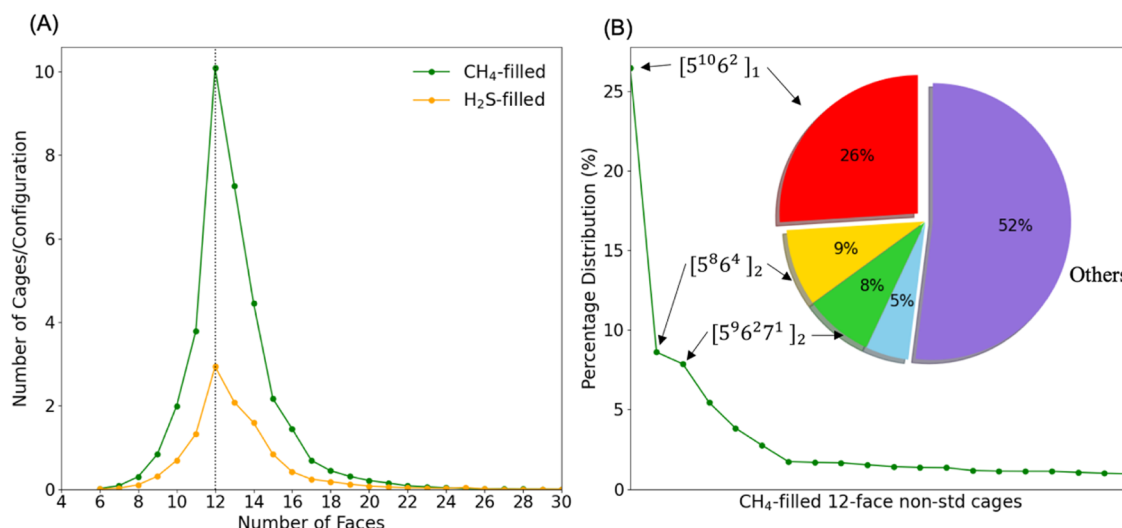


Figure 6. Properties of singly occupied nonstd cages for run 1 of sys-A with y_{CH_4} of 75% for the time period $t_{\text{relative}} = -59 \text{ ns}$ to $t_{\text{relative}} = 0$ for the trajectory corresponding to the black curve in Figure 2B. (A) Population distribution for nonstd cages per configuration with different numbers of faces. (B) Percentage distributions of CH_4 -filled 12-face nonstd cages, where only the top 20 cages in the distribution are presented. The percentage distribution for all 12-face nonstd cages is present in the inset chart, where the slices illustrate the percentages of the top 4 and all others in the system.

solution before and during the nucleation. However, if we focus on the mole ratios of $\text{CH}_4/\text{H}_2\text{S}$ in the hydrate phase and the aqueous phase, it is apparent in Figure 5D that the mole

ratio of $\text{CH}_4/\text{H}_2\text{S}$ is always higher in the hydrate phase. This observation of CH_4 -relative enrichment implies the formation of a CH_4 -rich hydrate phase from an aqueous phase relatively

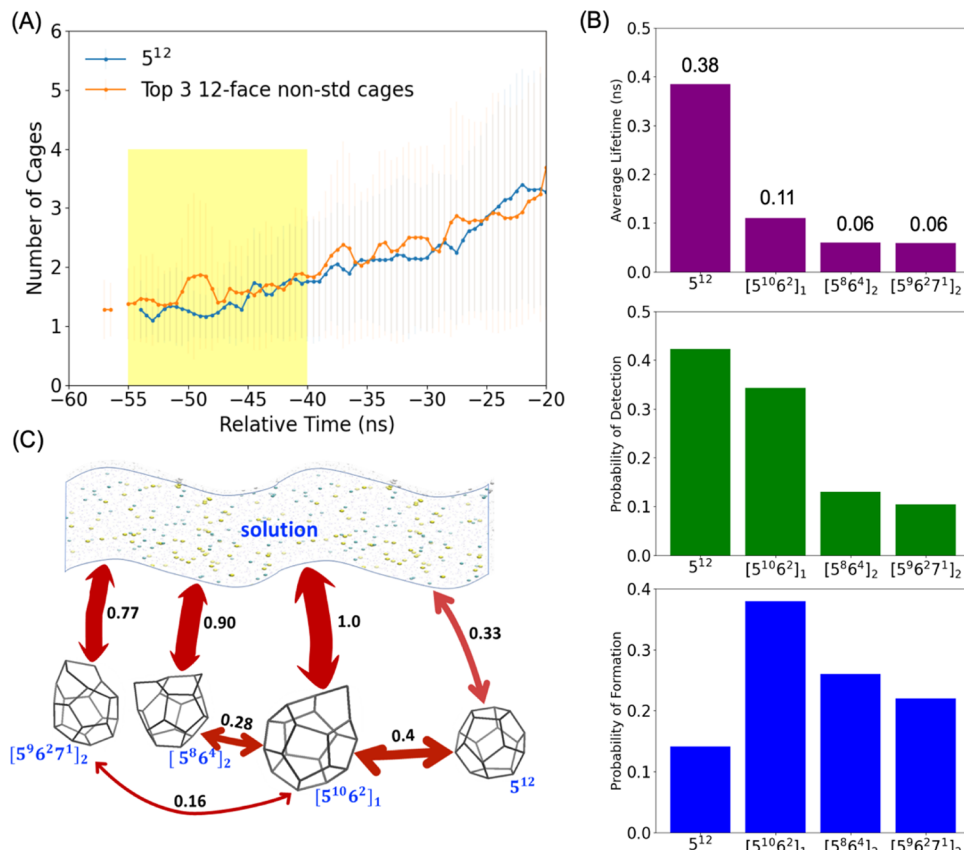


Figure 7. Twelve-face cage populations, lifetimes, and transitions. (A) Time evolution of number of singly occupied S^{12} and the three dominant 12-face nonstd cages of sys-A with y_{CH_4} of 75%. The error bars representing standard deviations are provided. The period used for calculating the lifetimes of the four cage types and their cage transitions is highlighted in yellow. (B) Average lifetime of the four cage types where the numbers at the top of each bar are the corresponding lifetimes (top), the relative probability of detection (middle), and the relative probability of formation (bottom). (C) Transition fluxes measured between the top three 12-face nonstd cages, S^{12} cages, and aqueous solution. The values associated with each arrow, whose width has also been scaled accordingly, are the fluxes normalized relative to the maximum flux value arising from the transition between aqueous solution and $[5^{10}6^2]_1$ cages. Only transitions with normalized fluxes greater than 0.05 are shown.

enriched in H_2S . With y_{CH_4} of 50 and 90% in sys-A, similar behavior can be found, where CH_4 is enriched in the hydrate phase, as presented in Figures S11 and S12. On average, increasing the system content of gas molecules does enhance the corresponding occupancy in the hydrate phase, whereas CH_4 always exhibits enrichment in the hydrate phase relative to the aqueous phase. These CH_4 -rich hydrate phases are comparable to the analogous CH_4/CO_2 nanobubble systems with $y_{CH_4} = 50\%$.⁶³ In this previous study, CH_4 -rich nuclei were obtained from a CO_2 -rich solution (e.g., see Figure 7 in ref 63); however, only standard hydrate cages were considered for their analysis.

For sys-B, it is important to note that it has an aqueous solution with the same initial concentration of CH_4 and H_2S ($x_{CH_4} = x_{H_2S} = 0.0318$). In this case, the distributions for the number of CH_4 - and H_2S -filled S^{12} cages tend to overlap (see Figure S13), whereas at a higher temperature, there appears to be a slight trend to favor CH_4 -filled S^{12} . On the other hand, the distributions for the number of CH_4 - and H_2S -filled nonstd cages consistently show the preferential uptake of CH_4 (see Figure S13), which is consistent with previous observations for hydrate nucleation within a CH_4/H_2S mixed system at 250 K and 50 MPa.⁴⁰ In this previous work, with $y_{CH_4} = 50\%$ showing a preferential uptake of CH_4 by nonstd cages, it was claimed

that the preferential enclathration of CH_4 was not a volume effect but the outcome of the guest–host interactions (e.g., the hydrogen bond between $H_2O \cdots H_2S$). We remark that in the current study, which is 10 K lower in temperature than the previous study with $y_{CH_4} = 50\%$ in sys-A, no apparently preferential uptake is observed. We conjecture that the formation of H_2S -filled cages is kinetically favored at a lower temperature, while CH_4 -filled cages are stabilized by increased temperature.

The dominance of nonstd cages in these systems brings forward another question: might there be any cage types ignored previously that play significant roles in hydrate formation? To further identify the primary cage types among nonstd cages, we calculate probability distributions of the number of faces for nonstd cages that are singly occupied by CH_4 or H_2S . These distributions are given in Figure 6A; we find that, as with std cages, nonstd cages with 12 faces predominate in the system. We then conjecture that there may be a large flux of transitions occurring between S^{12} cages and other 12-face nonstd cages, and that these nonstd cages may represent intermediate structures between that of the aqueous solution and the S^{12} cages.

To help explore this hypothesis, Figure 6B shows the percentage distribution of CH_4 -filled 12-face nonstd cages. We see that a relatively small number of specific nonstd cages tend

to dominate, namely, $[5^{10}6^2]_1$, $[5^86^4]_2$, and $[5^96^{27}]_2$ (where the subscript indicates the number of unsaturated vertices with only two edges) with percentages of 26, 9, and 8%, respectively. Interestingly, these three previously ignored cages consistently predominate in all other systems irrespective of the guest molecule and the specific conditions in the study.

To further test our hypothesis, Figure 7A reports the numbers of singly occupied 12-face cages, where we focus on S^{12} and the three most probable nonstd cages during early-stage nucleation. We see that the system initially contains primarily these nonstd cages, although eventually the number of S^{12} cages increases to exceed the populations of these nonstd cages and dominate the system. If we focus on the early stage of the nucleation (i.e., the yellow shaded region in Figure 7A), we can determine the average lifetime, the probability of formation, and the probability of detection in the specific configurations for the 4 cage types for this period (see the SI); we can also measure the transition fluxes between these 4 cage types and aqueous solution for 10 ps time windows. Interestingly, as shown in Figure 7B, the S^{12} cage has the largest values for both the lifetime and probability of detection, followed by $[5^{10}6^2]$, then $[5^86^4]_2$ and $[5^96^{27}]_2$, yet for the probability of formation, the $[5^{10}6^2]_1$ cage has the largest value, followed by $[5^86^4]_2$ and $[5^96^{27}]_2$, and the S^{12} cage has the smallest value. This indicates that these nonstd cages, particularly $[5^{10}6^2]_1$, apparently form more readily in comparison to S^{12} cages. However, the longer lifetime of the S^{12} cage, 0.38 ns, arising from its greater stability in comparison to the top three 12-face nonstd cages, apparently more than compensates and thus results in S^{12} cages having a somewhat higher probability of detection. Moreover, we can see from Figure 7C, where transition fluxes between these 4 cage types and aqueous solution are reported, that the $[5^{10}6^2]_1$ cage has the largest flux, followed by $[5^86^4]_2$ and $[5^96^{27}]_2$, and S^{12} has the smallest transition flux from the solution. This demonstrates that during early-stage nucleation the structural fluctuations in solution more readily give rise to 12-face nonstd cages compared to S^{12} cages, where the greater ease of formation of the more disordered structures presumably arises because of the smaller entropic penalties associated with their formation.⁶⁴ In addition, we note that the transition flux between $[5^{10}6^2]_1$ and S^{12} cages is significantly larger than that between solution and S^{12} . This confirms that the formation of a S^{12} cage via more disordered precursors, particularly $[5^{10}6^2]_1$, is the more frequent transition pathway. Thus, we can see that more disordered structures, represented by nonstd cages, can act as important intermediate structures leading to the formation of S^{12} cages from the solution.

These observations confirm our hypothesis that the 12-face nonstd cages can represent important precursors to S^{12} cages. To further understand the nature of the transition pathways among these nonstd cages and S^{12} , Figure 8 illustrates apparent mechanisms for these transitions. For example, by removal of one H_2O molecule, as shown in Figure 8, a $[5^{10}6^2]_1$ cage can transition into a S^{12} cage. In a $[5^{10}6^2]_1$ cage there are three types of edges, as indicated in Figure 8, edges that are (1) shared by two pentagonal faces, (2) shared by a pentagonal face and a hexagonal face, and (3) shared by two hexagonal faces. As a consequence, we can see that starting with a $[5^{10}6^2]_1$ cage, a $[5^86^4]_2$ cage forms by adding one H_2O molecule on a two-pentagon shared edge, or a $[5^96^{27}]_2$ cage forms by adding one H_2O molecule on a pentagon–hexagon shared edge. However, apparently due to the ring strain

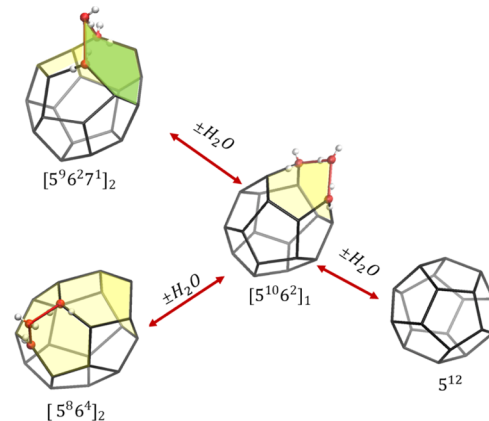


Figure 8. Schematic presentation of cage transition pathways between 12-face nonstd cages and a S^{12} cage. Cages are shown by black tubes where the heptagonal face is shaded green, and the hexagonal face is shaded yellow. The H_2O molecule added/removed and the H_2O molecules hydrogen-bonded to it are shown in a ball-and-stick representation, where oxygen is in red and hydrogen is in white.

introduced by adding a H_2O molecule on a hexagon–hexagon shared edge, $[5^{10}6^2]_2$ cages are relatively rare events. In the transition pattern described above, the $[5^{10}6^2]_1$ cage apparently acts as a transition hub located at the center of a transition network. Also, important to this analysis is the identification of a cage with a seven-number ring as being important in the structural transitions during hydrate formation (i.e., removal of two H_2O molecules from a $[5^96^{27}]_2$ cage can lead to a S^{12} cage, both with 12 faces).

We postulate that the possible transitions among various cages tend to preserve the number of faces, while transitions that change the number of faces are less frequent. This conjecture then implies that there should be a sequence (network) of transitions that links the disordered structure of the aqueous state to the crystalline hydrate phase, where nonstd cages before and during nucleation are important intermediates of a staged ordering process. Studies to probe this conjecture are currently underway.

Finally, let us consider the induction time, given that the average induction time has been frequently used as a measure of hydrate nucleation in both experimental and computational studies, although it is important to note that the two different methods typically sample very different timescales.^{1,3,43} To further examine the impact of the conditions on the formation of the hydrate phase, we define the induction time (τ) of hydrate nucleation for each trajectory as the time point at which the largest persistent cluster comprising more than two CCs appears. The evaluation of guest composition dependence of the induction time at a fixed temperature is presented in Figure 9A. The trend of the induction times for sys-A implies that a lower H_2S composition ($y_{H_2S} = 10\%$) slows down the hydrate formation, while the induction time is still comparable to pure H_2S cylindrical nanobubble systems at 240 K and 50 MPa (e.g., Figure 5 in ref 5) rather than to pure CH_4 nanobubble systems where the induction times of several hundreds of nanoseconds, or even longer, are required depending on the pressure–temperature conditions.^{12,16,17,20,21,65} This emphasizes that relatively small amounts of H_2S can strongly impact the rates of hydrate nucleation.

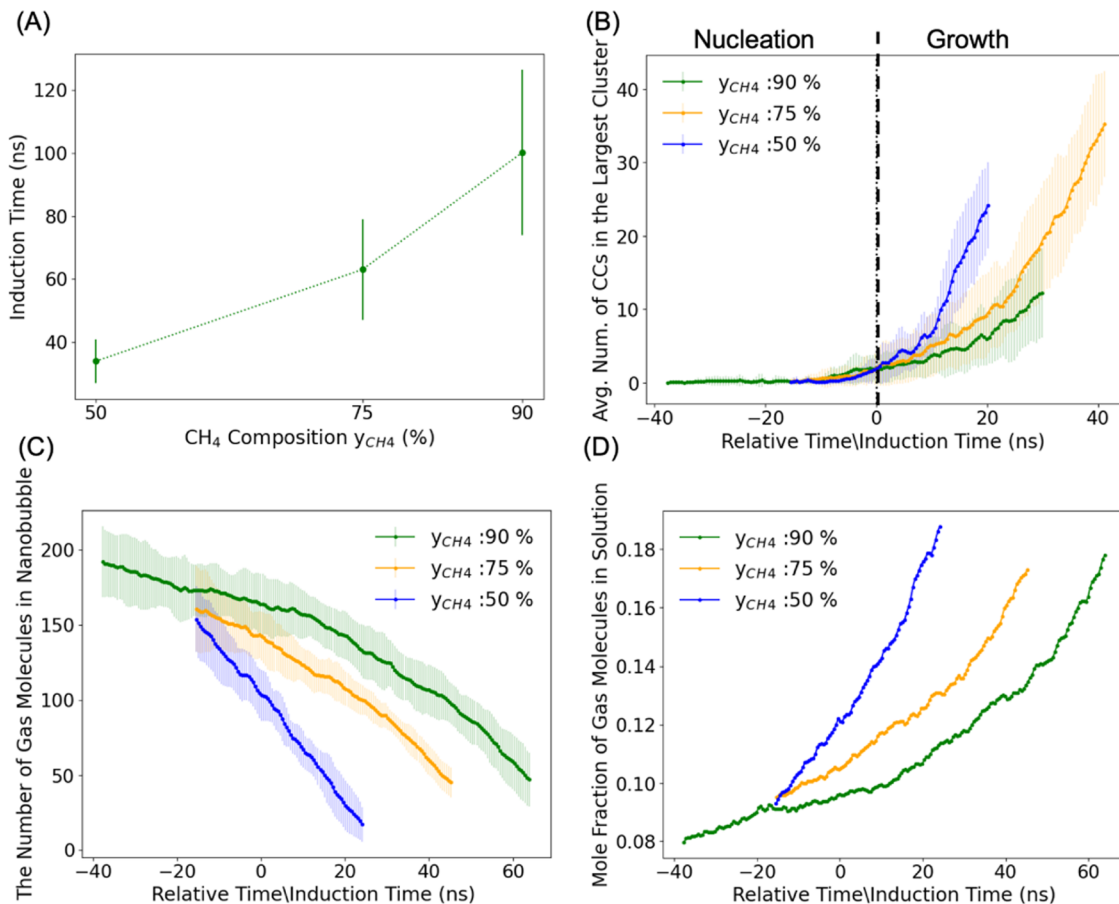


Figure 9. Composition impacts on gas hydrate nucleation in sys-A. (A) Average induction time. The green dashed line is to aid the eye. (B) Time evolution of the number of the CCs in the largest cluster for different compositions. (C) Time evolution of the total number of molecules in the guest nanobubble for different compositions. In panels (A)–(C), the error bars representing standard deviations are provided. (D) Total guest composition in an aqueous phase. Panels (B)–(D) use the $t_{\text{relative}/\text{induction}}$ timescale (see main text).

To further compare the composition dependence of the formation of the hydrate nuclei in an appropriate timescale, the nucleating trajectories have been shifted using the average induction time (see Figure S14), where we designate this as the relative/induction time ($t_{\text{relative}/\text{induction}}$). We assume that $t_{\text{relative}/\text{induction}} < 0$ corresponds to the nucleation stage, while $t_{\text{relative}/\text{induction}} > 0$ is the growth stage. With a higher content of H₂S in sys-A, the shorter duration for the nucleation stage and the steeper curve for the growth of nuclei are apparent, as shown in Figure 9. This indicates that the higher content of H₂S facilitates the rate for both nucleation and growth of the mixed hydrate. This rapid formation of nuclei is facilitated by the ability of H₂S to accelerate the shrinkage of the nanobubble and enhance the solubility of CH₄ molecules in the aqueous solution. As can be seen in Figure 9C,D, the time required for the shrinkage of the nanobubble decreases, and the total concentration in solution increases with the increase of y_{H_2S} . Additionally, with y_{H_2S} of only 10% (34 H₂S out of 340 total guest molecules) in sys-A, the total concentration of guests is boosted to a mole fraction of ~ 0.08 in the early quiescent period, which is about 1.7 times the critical concentration of CH₄ (0.045 ± 0.004) at 250 K.²³ The evaluation of the temperature dependence of the induction time at fixed guest composition is presented in Figure S15. An increased temperature does slightly increase the induction time; however, the temperature does not significantly impact the

rate of growth of nuclei in sys-B given the lower concentration in solution.

CONCLUSIONS

Extensive molecular dynamics (MD) simulations have been performed to probe the nucleation behavior of CH₄/H₂S mixed hydrate formation from two different system setups: (1) a guest nanobubble in an aqueous solution and (2) homogeneous solutions. Detailed analyses of the formation of cages in molecular simulations of CH₄/H₂S mixed hydrates with different compositions and different temperatures were performed to help reveal the underlying molecular mechanisms. We find that the order and appearance for the standard cages, where S^{12} cages are predominant, in accord with previous studies, are robust across the various conditions (i.e., compositions and temperatures) explored in this study. Nonstandard cages have been identified as dominating in populations before and during the early nucleation processes and appearing in the interfacial area between the hydrate phase and aqueous solution phases. Among the nonstandard cages, 12-face cages that are less symmetric and more irregular than S^{12} have been found as important intermediate structures in the nucleation process. Notably, we have demonstrated a network of key transitions among S^{12} , $[S^96^27^1]_2$, $[S^86^4]_2$, and $[S^{10}6^2]_1$ cages. Moreover, this transition pathway includes a novel cage type with a seven-number ring, namely, $[S^96^27^1]_2$. We propose that the mechanism of hydrate formation exhibits

patterns of transitions that are dominated by transitions occurring between cages with the same number of faces and where these transitions are apparently invariant to the physical setups and the parameters employed in the simulations. We have also found that the CH₄ species were always enriched in the hydrate phase relative to the aqueous solution across all systems, and that increasing H₂S composition can significantly enhance the rate of nucleation and growth of the hydrate formation through enhancement of the solubility of guests in solution.

The results in this investigation address several key aspects of hydrate nucleation, while also raising several other interesting questions that motivate future studies focused on further explorations of the mechanisms of cage transitions associated with hydrate nucleation and their corresponding thermodynamics characteristics. To help complete this molecular-level picture of hydrate nucleation, work aimed at applying more detailed stochastic models (e.g., Markov state models) to the various transitions between cage types during hydrate nucleation is currently underway.

ASSOCIATED CONTENT

Supporting Information

The Supporting Information is available free of charge at <https://pubs.acs.org/doi/10.1021/acs.jpcb.2c03223>.

Additional details of methods, supplementary figures for the nucleation process, temporal alignment strategy for sys-A and sys-B, supplementary figures for structures of the hydrate nuclei, supplementary figures for the composition of the hydrate nuclei, comparison of compositional dependence for sys-A, temperature dependence for sys-B, and analysis of lifetime are provided in the SI ([PDF](#))

AUTHOR INFORMATION

Corresponding Author

Peter G. Kusalik – Department of Chemistry, University of Calgary, Calgary T2N 1N4 Alberta, Canada;  orcid.org/0000-0001-6270-663X; Email: pkusalik@ucalgary.ca

Authors

Lei Wang – Department of Chemistry, University of Calgary, Calgary T2N 1N4 Alberta, Canada

Kyle Hall – Department of Chemistry, University of Calgary, Calgary T2N 1N4 Alberta, Canada; Present Address: Compliance Oversight of Models Office, TD Bank 79 Wellington St. West, Toronto, MSK 1A2 Ontario, Canada;  orcid.org/0000-0003-1611-7812

Zhengcai Zhang – Laboratory for Marine Mineral Resources, Pilot National Laboratory for Marine Science and Technology, Qingdao 266071, China;  orcid.org/0000-0001-5945-0303

Complete contact information is available at: <https://pubs.acs.org/10.1021/acs.jpcb.2c03223>

Notes

The authors declare no competing financial interest.

ACKNOWLEDGMENTS

The authors are grateful for the financial support of the Natural Sciences and Engineering Research Council of Canada (RGPIN-2016-03845). The authors thank Compute Canada

for computational resources. The authors also thank the Supercomputing Laboratory at IGGCAS and Center for High-Performance Computing and System Simulation, Pilot National Laboratory for Marine Science and Technology (Qingdao) for the allocation of computing time.

REFERENCES

- (1) Sloan, E. D.; Koh, C. A.; Koh, C. *Clathrate Hydrates of Natural Gases*, CRC Press: Boca Raton, FL, 2007.
- (2) Hassanpouryouzband, A.; Joonaki, E.; Vasheghani Farahani, M.; Takeya, S.; Ruppel, C.; Yang, J.; English, N. J.; Schicks, J. M.; Edlmann, K.; Mehrabian, H.; Aman, Z. M.; Tohidi, B. *Gas Hydrates in Sustainable Chemistry*. *Chem. Soc. Rev.* **2020**, *49*, 5225–5309.
- (3) Khurana, M.; Yin, Z.; Linga, P. *A Review of Clathrate Hydrate Nucleation*. *ACS Sustainable Chem. Eng.* **2017**, *5*, 11176–11203.
- (4) Veluswamy, H. P.; Kumar, A.; Seo, Y.; Lee, J. D.; Linga, P. *A Review of Solidified Natural Gas (SNG) Technology for Gas Storage via Clathrate Hydrates*. *Appl. Energy* **2018**, *216*, 262–285.
- (5) Cheng, Z.; Li, S.; Liu, Y.; Zhang, Y.; Ling, Z.; Yang, M.; Jiang, L.; Song, Y. *Post-Combustion CO₂ Capture and Separation in Flue Gas Based on Hydrate Technology: A Review*. *Renewable Sustainable Energy Rev.* **2022**, *154*, No. 111806.
- (6) Khan, M.; Warrier, P.; Peters, C.; Koh, C. *Hydrate-Based Separation for Industrial Gas Mixtures*. *Energies* **2022**, *15*, 966.
- (7) Dong, H.; Wang, J.; Xie, Z.; Wang, B.; Zhang, L.; Shi, Q. *Potential Applications Based on the Formation and Dissociation of Gas Hydrates*. *Renewable Sustainable Energy Rev.* **2021**, *143*, No. 110928.
- (8) Babu, P.; Nambiar, A.; He, T.; Karimi, I. A.; Lee, J. D.; Englezos, P.; Linga, P. *A Review of Clathrate Hydrate Based Desalination to Strengthen Energy-Water Nexus*. *ACS Sustainable Chem. Eng.* **2018**, *6*, 8093–8107.
- (9) Yin, Z.; Linga, P. *Methane Hydrates: A Future Clean Energy Resource*. *Chinese J. Chem. Eng.* **2019**, *27*, 2026–2036.
- (10) Mokhatab, S.; Wilkens, R. J.; Leontaritis, K. J. *A Review of Strategies for Solving Gas-Hydrate Problems in Subsea Pipelines*. *Energy Sources, Part A Recover. Util. Environ. Eff.* **2007**, *29*, 39–45.
- (11) Sosso, G. C.; Chen, J.; Cox, S. J.; Fitzner, M.; Pedevilla, P.; Zen, A.; Michaelides, A. *Crystal Nucleation in Liquids: Open Questions and Future Challenges in Molecular Dynamics Simulations*. *Chem. Rev.* **2016**, *116*, 7078–7116.
- (12) Walsh, M. R.; Koh, C. A.; Sloan, E. D.; Sum, A. K.; Wu, D. T. *Microsecond Simulations of Spontaneous Methane Hydrate Nucleation and Growth*. *Science* **2009**, *326*, 1095–1098.
- (13) Sarupria, S.; G Debenedetti, P. *Homogeneous Nucleation of Methane Hydrate in Microsecond Molecular Dynamics Simulations*. *J. Phys. Chem. Lett.* **2012**, *3*, 2942–2947.
- (14) Vatamanu, J.; Kusalik, P. G. *Observation of Two-Step Nucleation in Methane Hydrates*. *Phys. Chem. Chem. Phys.* **2010**, *12*, 15065.
- (15) Arjun; Berendsen, T. A.; Bolhuis, P. G. *Unbiased Atomistic Insight in the Competing Nucleation Mechanisms of Methane Hydrates*. *Proc. Natl. Acad. Sci. U.S.A.* **2019**, *116*, 19305–19310.
- (16) Walsh, M. R.; Beckham, G. T.; Koh, C. A.; Sloan, E. D.; Wu, D. T.; Sum, A. K. *Methane Hydrate Nucleation Rates from Molecular Dynamics Simulations: Effects of Aqueous Methane Concentration, Interfacial Curvature, and System Size*. *J. Phys. Chem. C* **2011**, *115*, 21241–21248.
- (17) Jiménez-Ángeles, F.; Firoozabadi, A. *Nucleation of Methane Hydrates at Moderate Subcooling by Molecular Dynamics Simulations*. *J. Phys. Chem. C* **2014**, *118*, 11310–11318.
- (18) Guo, G.-J.; Rodger, P. M. *Solubility of Aqueous Methane under Metastable Conditions: Implications for Gas Hydrate Nucleation*. *J. Phys. Chem. B* **2013**, *117*, 6498–6504.
- (19) Barnes, B. C.; Knott, B. C.; Beckham, G. T.; Wu, D. T.; Sum, A. K. *Reaction Coordinate of Incipient Methane Clathrate Hydrate Nucleation*. *J. Phys. Chem. B* **2014**, *118*, 13236–13243.

- (20) Yuhara, D.; Barnes, B. C.; Suh, D.; Knott, B. C.; Beckham, G. T.; Yasuoka, K.; Wu, D. T.; Sum, A. K. Nucleation Rate Analysis of Methane Hydrate from Molecular Dynamics Simulations. *Faraday Discuss.* **2015**, *179*, 463–474.
- (21) Knott, B. C.; Molinero, V.; Doherty, M. F.; Peters, B. Homogeneous Nucleation of Methane Hydrates: Unrealistic under Realistic Conditions. *J. Am. Chem. Soc.* **2012**, *134*, 19544–19547.
- (22) Lauricella, M.; Meloni, S.; J English, N.; Peters, B.; Ciccotti, G. Methane Clathrate Hydrate Nucleation Mechanism by Advanced Molecular Simulations. *J. Phys. Chem. C* **2014**, *118*, 22847–22857.
- (23) Bi, Y.; Porras, A.; Li, T. Free Energy Landscape and Molecular Pathways of Gas Hydrate Nucleation. *J. Chem. Phys.* **2016**, *145*, No. 211909.
- (24) Bi, Y.; Li, T. Probing Methane Hydrate Nucleation Through the Forward Flux Sampling Method. *J. Phys. Chem. B* **2014**, *118*, 13324–13332.
- (25) Zhang, Z.; Liu, C.-J.; Walsh, M. R.; Guo, G.-J. Effects of Ensembles on Methane Hydrate Nucleation Kinetics. *Phys. Chem. Chem. Phys.* **2016**, *18*, 15602–15608.
- (26) Zhang, Z.; Walsh, M. R.; Guo, G. J. Microcanonical Molecular Simulations of Methane Hydrate Nucleation and Growth: Evidence That Direct Nucleation to sI Hydrate is Among the Multiple Nucleation Pathways. *Phys. Chem. Chem. Phys.* **2015**, *17*, 8870–8876.
- (27) Zhang, Z.; Kusalik, P. G.; Guo, G.-J. Bridging Solution Properties to Gas Hydrate Nucleation Through Guest Dynamics. *Phys. Chem. Chem. Phys.* **2018**, *20*, 24535–24538.
- (28) Lauricella, M.; Ciccotti, G.; J English, N.; Peters, B.; Meloni, S. Mechanisms and Nucleation Rate of Methane Hydrate by Dynamical Nonequilibrium Molecular Dynamics. *J. Phys. Chem. C* **2017**, *121*, 24223–24234.
- (29) Liang, S.; Kusalik, P. G. Exploring Nucleation of H₂S Hydrates. *Chem. Sci.* **2011**, *2*, 1286–1292.
- (30) Liang, S.; Kusalik, P. G. Nucleation of Gas Hydrates within Constant Energy Systems. *J. Phys. Chem. B* **2013**, *117*, 1403–1410.
- (31) He, Z.; Linga, P.; Jiang, J. What Are the Key Factors Governing the Nucleation of CO₂ Hydrate? *Phys. Chem. Chem. Phys.* **2017**, *19*, 15657–15661.
- (32) Wilson, D. T.; Barnes, B. C.; Wu, D. T.; Sum, A. K. Molecular Dynamics Simulations of the Formation of Ethane Clathrate Hydrates. *Fluid Phase Equilib.* **2016**, *413*, 229–234.
- (33) Jiménez-Ángeles, F.; Firoozabadi, A. Enhanced Hydrate Nucleation Near the Limit of Stability. *J. Phys. Chem. C* **2015**, *119*, 8798–8804.
- (34) Yagasaki, T.; Matsumoto, M.; Tanaka, H. Formation of Clathrate Hydrates of Water-Soluble Guest Molecules. *J. Phys. Chem. C* **2016**, *120*, 21512–21521.
- (35) Yagasaki, T.; Matsumoto, M.; Tanaka, H. Mechanism of Slow Crystal Growth of Tetrahydrofuran Clathrate Hydrate. *J. Phys. Chem. C* **2016**, *120*, 3305–3313.
- (36) Jacobson, L. C.; Hujo, W.; Molinero, V. Amorphous Precursors in the Nucleation of Clathrate Hydrates. *J. Am. Chem. Soc.* **2010**, *132*, 11806–11811.
- (37) DeFever, R. S.; Sarupria, S. Nucleation Mechanism of Clathrate Hydrates of Water-Soluble Guest Molecules. *J. Chem. Phys.* **2017**, *147*, No. 204503.
- (38) He, Z.; Gupta, K. M.; Linga, P.; Jiang, J. Molecular Insights into the Nucleation and Growth of CH₄ and CO₂ Mixed Hydrates from Microsecond Simulations. *J. Phys. Chem. C* **2016**, *120*, 25225–25236.
- (39) Hall, K. W.; Carpendale, S.; Kusalik, P. G. Evidence From Mixed Hydrate Nucleation for a Funnel Model of Crystallization. *Proc. Natl. Acad. Sci. U.S.A.* **2016**, *113*, 12041–12046.
- (40) Hall, K. W.; Zhang, Z.; Kusalik, P. G. Unraveling Mixed Hydrate Formation: Microscopic Insights into Early Stage Behavior. *J. Phys. Chem. B* **2016**, *120*, 13218–13223.
- (41) Hall, K. W.; Zhang, Z.; Burnham, C. J.; Guo, G.-J.; Carpendale, S.; English, N. J.; Kusalik, P. G. Does Local Structure Bias How a Crystal Nucleus Evolves? *J. Phys. Chem. Lett.* **2018**, *9*, 6991–6998.
- (42) Wu, J. Y.; Chen, L. J.; Chen, Y. P.; Lin, S. T. Molecular Dynamics Study on the Nucleation of Methane + Tetrahydrofuran Mixed Guest Hydrate. *Phys. Chem. Chem. Phys.* **2016**, *18*, 9935–9947.
- (43) Zhang, Z.; Guo, G.-J.; Wu, N.; Kusalik, P. G. Molecular Insights into Guest and Composition Dependence of Mixed Hydrate Nucleation. *J. Phys. Chem. C* **2020**, *124*, 25078–25086.
- (44) Zhang, Z.; G Kusalik, P.; Guo, G.-J. Might a 2,2-Dimethylbutane Molecule Serve as a Site to Promote Gas Hydrate Nucleation? *J. Phys. Chem. C* **2019**, *123*, 20579–20586.
- (45) Scott, P. W.; Bristow, C. M.; London, G. S. of Industrial Minerals and Extractive Industry Geology: Based on Papers Presented at the Combined 36th Forum on the Geology of Industrial Minerals and 11th Extractive Industry Geology Conference, Bath, England, 7th–12th May, 2000; P. W., Scott; C M B, Ed.; Geological Society: Bath, England, 2002.
- (46) Leipert, G. F. Astrakhan, the World's Largest Sour Gas Development. *J. Can. Pet. Technol.* **1989**, *28* (DOI: [10.2118/89-03-11](https://doi.org/10.2118/89-03-11)).
- (47) Golombok, M.; Schoonebeek, R. Purification of Natural Gas by Forming H₂S Hydrates. *Energy Technol.* **2013**, *1*, 457–462.
- (48) Noaker, L. J.; Katz, D. L. Gas Hydrates of Hydrogen Sulfide–Methane Mixtures. *J. Pet. Technol.* **1954**, *6*, 135–137.
- (49) Ward, Z. T.; Marriott, R. A.; Sum, A. K.; Sloan, E. D.; Koh, C. A. Equilibrium Data of Gas Hydrates Containing Methane, Propane, and Hydrogen Sulfide. *J. Chem. Eng. Data* **2015**, *60*, 424–428.
- (50) Liang, H.; Duan, Y.; Pei, J.; Wei, N. Study on Hydrate Phase Equilibrium Diagram of Methane Containing System Based on Thermodynamic Model. *Front. Energy Res.* **2021**, *9*, 611.
- (51) Abascal, J. L. F.; Vega, C. A General Purpose Model for the Condensed Phases of Water: TIP4P/2005. *J. Chem. Phys.* **2005**, *123*, No. 234505.
- (52) Abascal, J. L. F.; Sanz, E.; García Fernández, R.; Vega, C. A Potential Model for the Study of Ices and Amorphous Water: TIP4P/Ice. *J. Chem. Phys.* **2005**, *122*, No. 234511.
- (53) Brooks, C. L. Computer Simulation of Liquids. *J. Solution Chem.* **1989**, *18*, 99.
- (54) Jorgensen, W. L.; Madura, J. D.; Swenson, C. J. Optimized Intermolecular Potential Functions for Liquid Hydrocarbons. *J. Am. Chem. Soc.* **2002**, *106*, 6638–6646.
- (55) Forester, T. R.; McDonald, I. R.; Klein, M. L. Intermolecular Potentials and the Properties of Liquid and Solid Hydrogen Sulphide. *Chem. Phys.* **1989**, *129*, 225–234.
- (56) Conde, M. M.; Gonzalez, M. A.; Abascal, J. L. F.; Vega, C. Determining the Phase Diagram of Water from Direct Coexistence Simulations: The Phase Diagram of the TIP4P/2005 Model Revisited. *J. Chem. Phys.* **2013**, *139*, No. 154505.
- (57) Liang, S.; Kusalik, P. G. Crystal Growth Simulations of H₂S Hydrate. *J. Phys. Chem. B* **2010**, *114*, 9563–9571.
- (58) Liang, S.; Rozmanov, D.; Kusalik, P. G. Crystal Growth Simulations of Methane Hydrates in the Presence of Silica Surfaces. *Phys. Chem. Chem. Phys.* **2011**, *13*, 19856–19864.
- (59) Rodger, P. M.; Forester, T. R.; Smith, W. Simulations of the Methane Hydrate/Methane Gas Interface near Hydrate Forming Conditions. *Fluid Phase Equilib.* **1996**, *116*, 326–332.
- (60) Guo, G.-J.; Zhang, Y.-G.; Liu, C.-J.; Li, K.-H. Using the Face-Saturated Incomplete Cage Analysis to Quantify the Cage Compositions and Cage Linking Structures of Amorphous Phase Hydrates. *Phys. Chem. Chem. Phys.* **2011**, *13*, 12048–12057.
- (61) Gillis, K.; Vatamanu, J.; Razul, M. S. G.; Kusalik, P. G. Averaged Configurations from Molecular Dynamics Simulations. In *Applied Parallel Computing. State of the Art in Scientific Computing*, Kågström, B.; Elmroth, E.; Dongarra, J.; Waśniewski, J., Eds.; Springer: Berlin Heidelberg, 2007; pp 51–58.
- (62) Walsh, M. R.; Rainey, J. D.; Lafond, P. G.; Park, D.-H.; Beckham, G. T.; Jones, M. D.; Lee, K.-H.; Koh, C. A.; Sloan, E. D.; et al. The Cages, Dynamics, and Structuring of Incipient Methane Clathrate Hydrates. *Phys. Chem. Chem. Phys.* **2011**, *13*, 19951–19959.

- (63) Yi, L. Z.; Liang, D. Q.; Zhou, X. B.; Li, D. L. Molecular Dynamics Simulations for the Growth of CH₄-CO₂ Mixed Hydrate. *J. Energy Chem.* **2014**, *23*, 747.
- (64) Liang, S.; Hall, K. W.; Laaksonen, A.; Zhang, Z.; Kusalik, P. G. Characterizing Key Features in the Formation of Ice and Gas Hydrate Systems. *Philos. Trans. R. Soc. A Math. Phys. Eng. Sci.* **2019**, *377*, No. 20180167.
- (65) Zhang, Z.; Guo, G.-J. The Effects of Ice on Methane Hydrate Nucleation: A Microcanonical Molecular Dynamics Study. *Phys. Chem. Chem. Phys.* **2017**, *19*, 19496–19505.